

A Comprehensive Study of the ^3He - ^4He II Sandwich System Using Monte Carlo Techniques

Amer Al-Oqali,¹ Asaad R. Sakhel,² and Humam B. Ghassib¹

¹*Department of Physics, Faculty of Science, The University of Jordan, Amman, JORDAN*

²*Faculty of Engineering Technology, Al-Balqa Applied University Amman 11134, JORDAN*

(Dated: May 29, 2022)

We present a numerical investigation of the thermal and structural properties of the ^4He - ^3He sandwich system adsorbed on a graphite substrate using the Worm Algorithm Quantum Monte Carlo (WAQMC) method [1]. For this purpose, we modified a previously written WAQMC code originally adapted for ^4He on graphite, by including the second ^3He -component. In order to describe the fermions, a temperature-dependent statistical potential was used which proved very effective. To the best of our knowledge, the statistical potential has not been used before in Quantum Monte Carlo techniques for describing fermions. In an unprecedented task, the WAQMC calculations were conducted in the milli-Kelvin temperature regime. However, because of the heavy computations involved, only 30, 40, and 50 mK were considered for the time being. The pair correlations, Matsubara Green's function, structure factor, and density profiles were explored at these temperatures. (Note: this paper is just a preliminary version and will be replaced by an updated version.)

I. INTRODUCTION

There have been only a few investigations on the ^4He - ^3He sandwich system in the last 25 years [2, 3], most of the studies having concentrated on ^4He - ^3He films [4–8] and superfluid ^4He films [9, 10]. These investigations aimed at calculating the Fermi liquid parameters, the speed of third sound in He II, the specific heat capacity, and the Kosterlitz-Thouless (KT) transition. ^4He - ^3He mixtures and films [11, 12] are considered important physical systems for several reasons: 1) their use in cooling to the milli-Kelvin regime; 2) the central role as theoretical labs for the study of a number of methods in many-body physics; and 3) the importance of the sandwich system specifically in its role where dimensionality effects arise. One can thus see the importance of this study, particularly since it will be conducted using Quantum Monte Carlo techniques. Previous work on ^4He - ^3He mixtures and films is abundant. Experimentally, the torsional oscillator was used to study the superfluid ^4He - ^3He sandwich system [13] and it was found that the critical temperature for the Kosterlitz-Thouless (KT) transition decreases as the number of ^3He atoms is increased. Measurements on third sound in ^4He - ^3He films have also been conducted. It was found that by increasing the concentration of ^3He in ^4He , the speed of third sound decreases and a complete phase separation occurs at $T \leq 0.5$ K. As a result, this system resembles the ^4He - ^3He sandwich system. Ghassib and Waqqad [14] reconsidered Bose-Einstein condensation in an ideal, quasi two-dimensional Bose gas and explored crossover effects from two- to three-dimensional systems. Further, Ghassib and Chatterjee [12] examined the effects of ^4He impurities on some low-temperature properties of normal liquid ^3He . It was argued that no ^4He - ^3He mixtures can possibly exist at very low temperature ($T \leq 100$ mK), where a total phase separation occurs.

From another point of view, the possibility for dimer

and trimer formation in ^4He - ^3He films was explored. Ghassib [8] predicted that dimers form initially in ^3He ; afterwards –at much lower temperatures– a KT transition could occur for boson composites. ^4He - ^3He mixtures in two dimensions have also been considered. For example Krotscheck *et al.* [11] showed that an effective interaction between pairs of ^3He atoms inside a host ^4He liquid was sufficient to cause loosely-bound dimers.

Investigations of ^4He on a graphite substrate have also been conducted. For example, Corboz *et al.* [15] investigated the low-temperature phase diagram of the first and second layer of ^4He adsorbed on graphite, using the worm algorithm. Pierce and Manousakis [9, 10] presented a path-integral Monte Carlo (PIMC) method for simulating helium films on the graphite surface, and investigated helium layers adsorbed on the substrate. In addition, diffusion Monte Carlo has also been used to study the first layer of ^4He adsorbed on graphite [16], and the ground-state properties of the homogeneous two-dimensional liquid ^4He [17].

It is obvious that these previous investigations are not enough; here we provide a more comprehensive in depth microscopic study of this system. Our chief goal is to compute some thermal and structural properties of the ^4He - ^3He sandwich system in the milli Kelvin temperature regime using the Worm Algorithm Quantum Monte Carlo method [1]. To the best of our knowledge, this kind of system has not been simulated before in such a low-temperature regime. Because of the heavy computational aspect of the present simulations, we were only able to obtain results for three temperatures: $T = 30, 40,$ and 50 mK.

The ^4He - ^3He sandwich system proper consists of a ^4He solid layer of $\sim 3.6\text{\AA}$ thickness adsorbed on the walls of a container, above which resides a ^4He - ^3He mixture-layer of $7\text{-}11\text{\AA}$ thickness followed by a pure bulk liquid ^3He layer. In this paper, we rejuvenate the investigations on this sandwich system which promises richness

in physics. We chiefly investigate the thermal properties, such as the pressure, internal energy, entropy, and superfluid density. By using the superfluid density one can detect the role of ^3He atoms in the depletion of the superfluid in such a many-body system. In addition, other properties can be obtained such as the solubility of ^3He into ^4He , and the density profiles which show layer promotion upon increasing the number of ^3He or ^4He atoms. Further, the Matsubara Green's function $G(p, \tau)$ [18] is computed by the numerical implementation of the WAQMC code [1] in order to check for excitations and particle propagation in the sandwich system. Another key point is that we use a statistical potential [19] in order to include real fermionic statistics into the calculations, thereby circumventing the fermion sign problem, which would otherwise arise if we allowed sign-changes corresponding to permutations of the fermions.

We thus consider N ^3He and ^4He atoms with different numeric ratios in a ^4He - ^3He sandwich system on graphite. The interactions between the ^4He atoms and the ^4He - ^3He pairs are described by the Aziz potential [20]; whereas the ^3He atoms interact by the fictitious statistical potential. The Worm-Algorithm Quantum Monte Carlo (WAQMC) method [1] is used to simulate this system. For this purpose, we modified a previously written Worm-Algorithm code [21] specifically designed for ^4He on graphite, by including a second component (^3He) into the code. The use of a statistical potential in the description of fermions in a Monte Carlo simulation is unprecedented, and we hope to be able to convince the reader of its effectiveness.

We found chiefly that the statistical potential is very effective in describing the ^3He fermions in a ^4He environment. The pair correlation function reveals strong correlations between the three pairs of ^3He - ^3He , ^4He - ^4He , and ^4He - ^3He atoms, signalling the presence of different types of clusters. The Matsubara Green's function demonstrated substantial activity in the system and a condensate fraction as well. The integrated density profiles, taken in a plane perpendicular to the substrate, revealed crystallization of the layers closest to the graphite substrate; whereas disorder is prevalent in the layers farther away from the substrate.

The organization of the paper is as follows. In Sec.II we describe the changes we made in the WAQMC code so as to include the ^3He component. For this purpose, we needed to recast some of the information in Ref.[1], so that the reader can understand our changes. In Sec.III we present the results of our calculations and discuss them. Finally, in Sec.IV we present our conclusions.

II. METHOD

In this section, we do not explain the WAQMC technique; we only outline our modifications to the code. The WAQMC method has been explained in detail by the inventors of the technique [1]. This technique is relatively new and based on conventional path integral Monte

Carlo (PIMC) described earlier by the excellent review of David Ceperley [22]. The idea behind the WAQMC method was to make PIMC more efficient by introducing off-diagonal configurations (worms) into the system in addition to the existing diagonal ones. That is, in WAQMC one uses configurations containing both closed (diagonal) world-lines and *one* open (off-diagonal) world-line (worm). The diagonal configurations contribute to the partition function, hence referred to as the Z -sector, whereas the off-diagonal ones to the Matsubara Green's function, G , hence referred to as the G -sector [1]. In PIMC as well as WAQMC, each particle is represented by a trajectory in space-time which closes upon itself in space after it has moved for a time β . Each position in space-time on this trajectory is represented by a bead, and each pair of consecutive beads is separated by a time slice τ . If there are M time slices, then $\beta = M\tau$, where M is the number of time slices along a certain trajectory, the path of the particle in space-time. The particle is thus described by a ring-polymer, an entirely new picture [22].

A. Interactions

For the ^4He - ^4He and ^4He - ^3He interactions, the standard interatomic Aziz potential [20] was used. For the ^3He - ^3He interactions we invoked a fermionic statistical potential [19] given by

$$v_s(r) = -k_B T \ln[1 - \exp(-2\pi r^2/\lambda^2)], \quad (1)$$

where $\lambda = \hbar^2/(2m)$, k_B being Boltzmann's constant, r the distance between a pair of ^3He atoms, and T the temperature. The idea behind the statistical potential is to simulate real fermions; thereby circumventing the sign problem, as mentioned previously.

B. Worm updates

In what follows, we describe the changes that we implemented in the WAQMC code in order to include the second ^3He component. For this purpose, we recast some of the information in Ref.[1] in order to shed enough light on the changes. All the worm-update equations and concepts used in this paper were given earlier in Ref.[1], except for the indicated changes made to accommodate the ^3He component.

The worm updates are accepted or rejected according to certain, carefully defined probabilities. In essence, only *one* worm is allowed and added to the diagonal configurations. This worm, when inserted, has a starting bead named for historical reasons *Masha* (\mathcal{M}), and an ending bead named *Ira* (\mathcal{I}). *Ira* always advances *Masha* in time. *Ira* or *Masha*, that is the end-beads of a worm, can be moved forward or backward in time. They can be reconnected to diagonal trajectories after these trajectories are cut open, and they can also close an off-diagonal

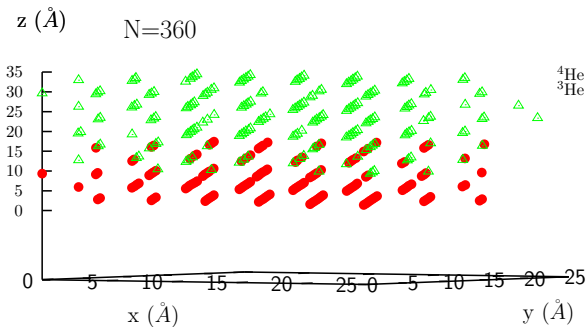


FIG. 1: Initialization of a ${}^4\text{He}$ - ${}^3\text{He}$ sandwich system of $N = 360$ atoms on a graphite substrate. The ${}^4\text{He}$ atoms (red circles) are adsorbed on a graphite surface constituting a layer of $\sim 3.6\text{\AA}$ thickness. The ${}^3\text{He}$ atoms (green triangles) form a bulk layer of about $\sim 7\text{\AA}$ thickness. Sandwiched in between these two is a ${}^4\text{He}$ - ${}^3\text{He}$ mixture-layer of $\sim 15\text{\AA}$ thickness. The ratio of ${}^3\text{He}$ and ${}^4\text{He}$ atoms in the latter is chosen randomly.

trajectory by glueing a worm to the opening. Further, a worm can be erased and then reintroduced. Beads across two different trajectories can be linked together by diagrammatic links, leading to bonds between them.

The WAQMC code was originally written [1] for one component only, namely ${}^4\text{He}$, on graphite. To include the ${}^3\text{He}$ component, a logical array *who_are_you*(bead) was introduced which would return a *true* value for a chosen bead if it was ${}^4\text{He}$, and *false* if it was ${}^3\text{He}$ in order to label the particles and to distinguish between them.

1. Initialization

The ${}^4\text{He}$ - ${}^3\text{He}$ sandwich system is initialized using straight world-lines each of length β as shown in Fig.1, for a system of, e.g., $N_3 = 222$ ${}^3\text{He}$ atoms and $N_4 = 138$ ${}^4\text{He}$ atoms. A logical bead list *who_are_you*(bead) is initialized as the sandwich system is built up into layers on graphite. The first layer adsorbed on the graphite surface consists of ${}^4\text{He}$ atoms only constituting about 25% of the total number of atoms N ($0.25\beta/\epsilon$ beads), the second consists of a ${}^4\text{He}$ - ${}^3\text{He}$ mixture constituting 25% of N , whereas the third layer consists only of ${}^3\text{He}$ atoms constituting the rest of N . Here, ϵ is the “time step” in the Worm Algorithm technique. The type of the atoms in the mixture-layer is randomly assigned to simulate a realistically mixed layer.

2. Insert

A worm, either fermionic or bosonic, is created as shown in Fig.2, where the beginning of the worm is *Masha* (\mathcal{M}) and the end *Ira* (\mathcal{I}). The figure is a presentation of the open (off-diagonal) trajectory in space-time. The type is assigned randomly using a certain probability: If a random number, $\xi < 0.5$ say, the mass used in the

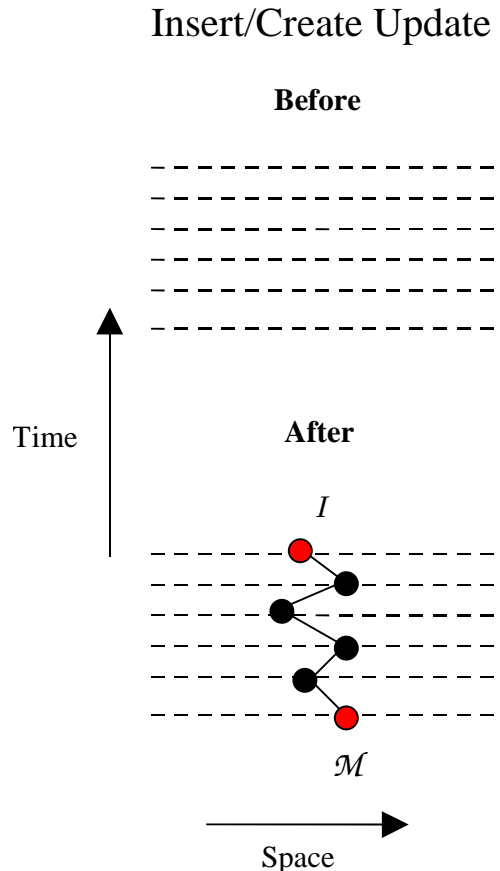


FIG. 2: Worm-Algorithm Insert update representation in space-time coordinates. *Ira* (\mathcal{I}) and *Masha* (\mathcal{M}) are shown as red solid circles.

updates will be that of ${}^4\text{He}$; if $\xi \geq 0.5$, the mass is that of ${}^3\text{He}$. Accordingly, we use in FORTRAN 90

$$\begin{aligned}
 &\xi = \text{rndm}() \\
 &\text{IF}(\xi \text{ .lt. } 0.5)\text{THEN} \\
 &\quad mp = m4 \\
 &\text{ELSEIF}(\xi \text{ .ge. } 0.5)\text{THEN} \\
 &\quad mp = m3 \\
 &\text{ENDIF}
 \end{aligned} \tag{2}$$

where mp is the mass variable in the program, and $m3$ and $m4$ are the masses of ${}^3\text{He}$ and ${}^4\text{He}$. In the upcoming types of worm updates, the beads, newly created or removed, are assigned the value **.TRUE.** or **.FALSE.**, respectively, according to the choice of the mass in the INSERT update above. Thus except for the CUT update (see Sec.II B 9 below), the types of beads and the associated mass used is the same as that chosen initially in the INSERT update.

The acceptance probability for this INSERT update is (as in Ref.[1])

$$P_{in} = \min \{1, 2CVPM e^{\Delta U + \mu M \epsilon}\}, \quad (3)$$

where ΔU is the change in the configurational potential energy of the beads due to the insertion of the worm, μ the chemical potential, and ϵ is the time step. Here, C is a constant, V the volume of the system, M the length of the worm proposed which is selected randomly within an interval $[1, \overline{M}]$, and $P = \beta/\epsilon$ is the number of time slices along the path of “length” β . In the WAQMC code, P_{in} is programmed as follows:

$$P_{in} = w_{ST} \cdot w_t \cdot V \frac{\beta}{2} \frac{\overline{M}}{2} \frac{p_{re}}{p_{in}} e^{\mu \epsilon M + \Delta U}, \quad (4)$$

where, w_{ST} controls the worm statistics, p_{re} and p_{in} are fixed attempt probabilities for removing and inserting a worm, respectively, and w_t is a weight determined from the total number of beads before and after an update. We multiplied Eqs.(4) and (6) below by $1/p_f$ or $1/p_b$ for a fermion or boson worm, respectively, where p_f is the attempt probability for getting a fermion and $p_b = 1 - p_f$ the attempt probability for getting a boson.

3. Remove

A worm, either fermion or boson, is removed (annihilated) as shown in Fig.3. The type of worm to be removed depends on the mass mp chosen in the INSERT update above. That is, if $mp = m3$, then a fermion worm is removed, otherwise if $mp = m4$ a boson worm. The probability for this update is

$$P_{rm} = \min \left\{ 1, \frac{e^{\Delta U - \mu \overline{M} \epsilon}}{2CVPM} \right\}, \quad (5)$$

and in the WAQMC program it is coded

$$P_{rm} = \frac{4 w_t e^{-\mu \epsilon \overline{M} + \Delta U} p_{in}}{w_{ST} \cdot V \cdot \beta \overline{M} p_{re}}. \quad (6)$$

As a preventive measure during the process of removing the beads, if at any time a bead to be removed has a different type than the worm beads on which the update is performed, the program terminates. But this is just in case and is not supposed to happen.

4. Move Forward Masha

In this update, the beginning of the worm (timewise speaking slice number 0) is propagated backwards in time as shown in Fig.4. That is to say, a chain of new beads is attached to the old *Masha* backwards in time ending then

Remove Update

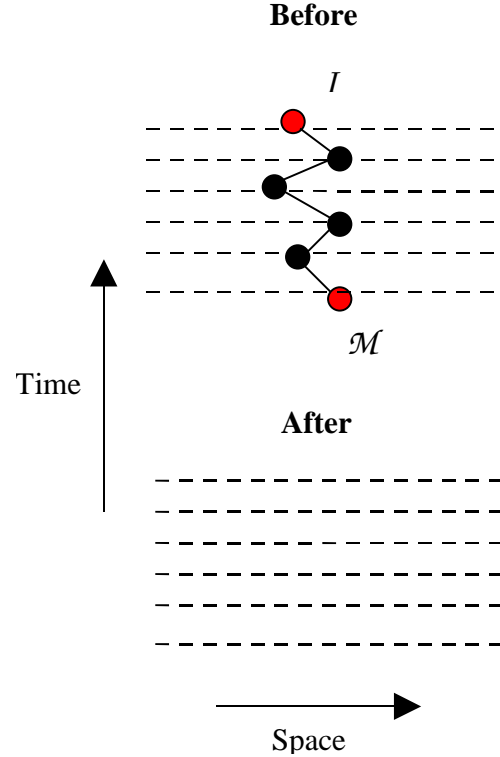


FIG. 3: As in Fig.2; but for the removal of a worm.

with a new *Masha*. The old *Masha* is then relabelled as an ordinary bead. In the event that a newly generated bead has a different type than *Masha* the program terminates according to the code:

IF(who_are_you(bead).ne.who_are_you(\mathcal{M}))STOP (7)

The type of the worm is pre-determined in the INSERT update. The probability for this update advancing *Masha* forward is

$$P_{ad, \mathcal{M}} = \min \{1, e^{-\Delta U + \mu M \epsilon}\}, \quad (8)$$

and in the program it is coded

$$P_{ad, \mathcal{M}} = e^{\mu \epsilon \overline{M} - \Delta U} \cdot w_t \cdot w_{lc, \mathcal{M}}. \quad (9)$$

Here $w_{lc, \mathcal{M}}$ is the worm-link correction of the links to *Masha* (\mathcal{M}):

$$w_{lc, \mathcal{M}} = \prod_{i=1}^{N_\ell} \left(\frac{e^{-\epsilon V(|\mathbf{r}_{\mathcal{M}} - \mathbf{r}_i|)} - 1}{e^{-\epsilon V(|\mathbf{r}_{\mathcal{M}} - \mathbf{r}_i|)/2} - 1} \right), \quad (10)$$

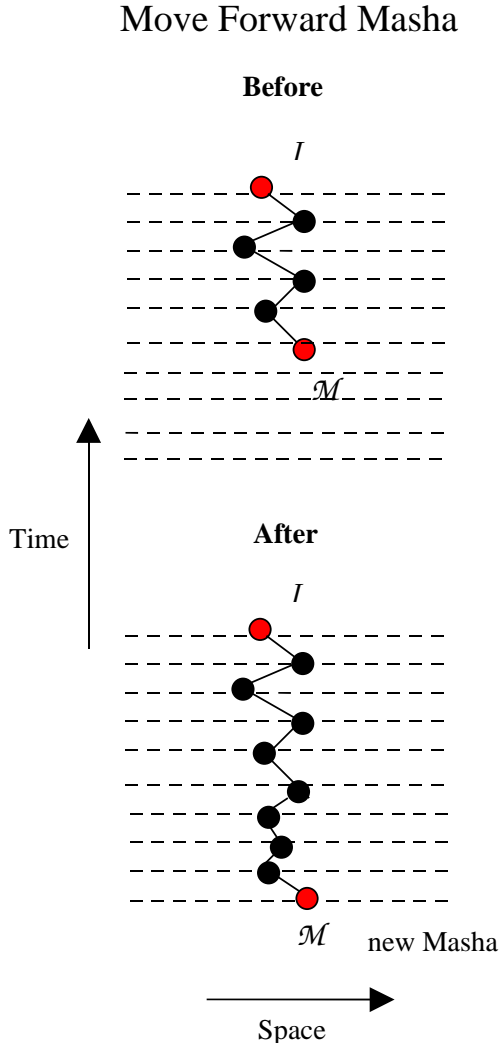


FIG. 4: Worm Algorithm update for moving *Masha* forward

where $r_{\mathcal{M}}$ is the position of *Masha*, \mathbf{r}_i the position of the bead i linked to *Masha*, N_{ℓ} is the number of links to *Masha*, and $V(r)$ is the pair interaction potential. Here, it doesn't matter what type of bead one links to since nothing prevents the formation of bonds between fermions and bosons.

5. Move Forward Ira

In this update, the end of the worm (timewise speaking last slice on worm) is propagated forward in time as in Fig.5. Again, the type of worm is pre-determined in the INSERT update, and any newly created beads must have the same type as that of the worm to be updated. If it happens that a bead has a different type than the worm, the program terminates according to

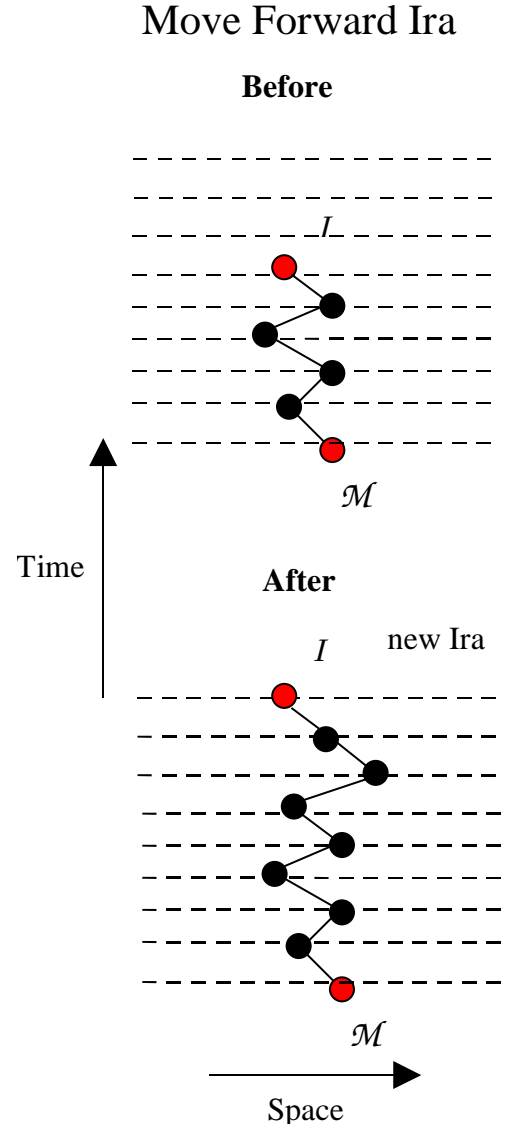


FIG. 5: Worm Algorithm update for moving *Ira* forward.

IF(*who_are_you*(bead).ne.*who_are_you*(\mathcal{I}))**STOP**.
(11)

The probability for this update is

$$P_{ad,\mathcal{I}} = \min \{1, e^{-\Delta U + \mu M \epsilon}\}, \quad (12)$$

and is coded

$$P_{ad,\mathcal{I}} = e^{\mu \epsilon \bar{M} - \Delta U} \cdot w_t \cdot w_{l_{c\mathcal{I}}}. \quad (13)$$

Here $w_{l_{c\mathcal{I}}}$ is the worm link correction of all the links to *Ira*

$$w_{lc_{\mathcal{I}}} = \prod_{i=1}^{N_{\ell}} \left(\frac{e^{-\epsilon V(|\mathbf{r}_{\mathcal{I}} - \mathbf{r}_i|)} - 1}{e^{-\epsilon V(|\mathbf{r}_{\mathcal{I}} - \mathbf{r}_i|)/2} - 1} \right), \quad (14)$$

where $\mathbf{r}_{\mathcal{I}}$ is the position of \mathcal{I} and N_{ℓ} is the number of links to \mathcal{I} .

6. Move Backward Masha

Here *Masha* is moved forward in time as in Fig.6. In other words, a chain of new beads is erased forward in time beginning with the old *Masha* until the erasure stops at a new worm-beginning which becomes then the new *Masha*. The probability of this update is

$$P_{re, \mathcal{M}} = \min \{1, e^{\Delta U - \mu M \epsilon}\}, \quad (15)$$

and is coded

$$P_{re, \mathcal{M}} = e^{-\mu \epsilon M + \Delta U} w_{lc, \mathcal{M}} \cdot w_t. \quad (16)$$

As a safety measure, any bead which has a different type than \mathcal{M} causes the program to stop, as in (7).

7. Move Backward Ira

This update moves *Ira* backward in time as in Fig.7. Correspondingly, a chain of beads is erased backwards in time beginning with the old *Ira* until the erasure stops at a new *Ira*. The resulting end of the worm becomes the new *Ira*. The probability is given by

$$P_{re, \mathcal{I}} = \min \{1, e^{\Delta U - M \epsilon \mu}\}, \quad (17)$$

and is coded:

$$P_{re, \mathcal{I}} = e^{-\mu \epsilon M + \Delta U} \cdot w_t \cdot w_{lc, \mathcal{I}}. \quad (18)$$

Again, if a bead happens to have a different type than \mathcal{I} , the program terminates as in (7) as a safety measure.

8. Glue

Here, a worm of a type chosen in the INSERT update, is closed to become a ring polymer as shown in Fig.8. *Masha* and *Ira* become ordinary beads in this case. The probability for this update is

$$P_{glue} = \min \left\{ 1, \frac{\rho_0(\mathbf{r}_{\mathcal{I}}, \mathbf{r}_{\mathcal{M}}, M \epsilon) e^{\Delta U + \mu M \epsilon}}{C \bar{M} N_{bd}} \right\}, \quad (19)$$

Move Backward Masha Update

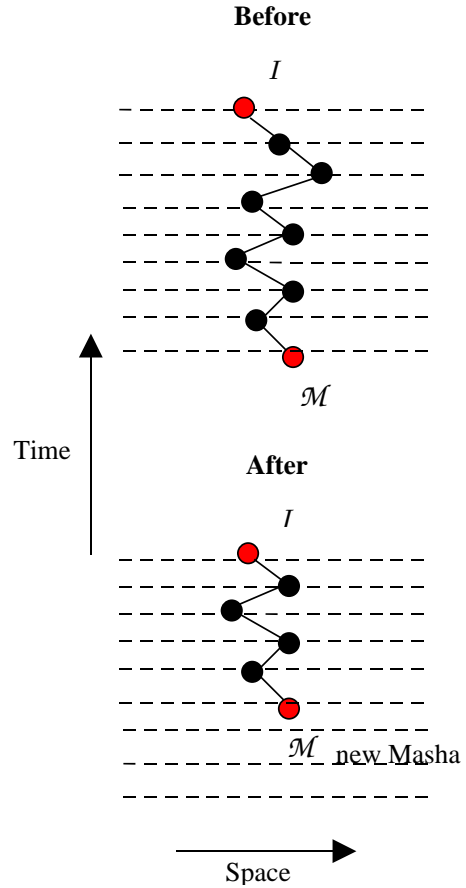


FIG. 6: As in Fig.4; but for moving *Masha* backward

where $\mathbf{r}_{\mathcal{I}}$ and $\mathbf{r}_{\mathcal{M}}$ are the positions of \mathcal{I} and \mathcal{M} , respectively, and N_{bd} is the current total number of beads. The free-particle propagator ρ_0 is given by

$$\rho_0(\mathbf{r}_{\mathcal{I}}, \mathbf{r}_{\mathcal{M}}, M \epsilon) = e^{-(\mathbf{r}_{\mathcal{I}} - \mathbf{r}_{\mathcal{M}})^2 / (4M \lambda \epsilon)}. \quad (20)$$

Eq.(19) is coded

$$P_{glue} = \left[\frac{1}{4} e^{-\mu \epsilon M + \Delta U} e^{-(\mathbf{r}_{\mathcal{I}} - \mathbf{r}_{\mathcal{M}})^2 \frac{mp}{2\epsilon \bar{M}}} (aM)^{3/2} (N_{bd} + M - 1) w_{ST} \bar{M} \frac{p_{gl}}{p_{cut}} w_{lc, \mathcal{I}} \cdot w_{lc, \mathcal{M}} \cdot w_t \right]^{-1},$$

where $a = 2\pi\epsilon/mp$, $\mathbf{r}_{\mathcal{I}}$ and $\mathbf{r}_{\mathcal{M}}$ are the positions of \mathcal{I} and \mathcal{M} , p_{gl} and p_{cut} are the probabilities for attempting a glue or a cut, respectively. The cutting procedure is explained in the next section below. Again, the glue beads must have the same type as the worm beads to be glued, otherwise the program stops using the Fortran statements similar to (7) or (11).

Move Backward Ira Update

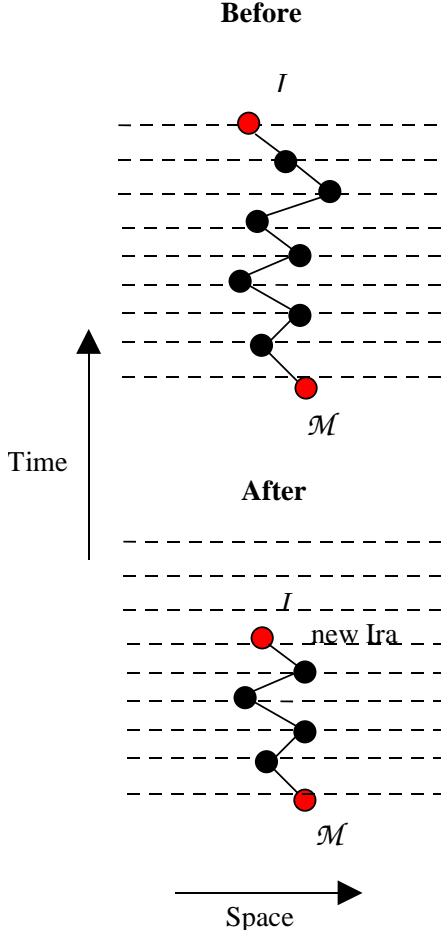


FIG. 7: As in Fig.5; but for moving *Ira* backward.

9. Cut

In this update, a randomly chosen piece of trajectory is removed from a ring polymer in order to create a worm as shown in Fig.9. The beginning of the worm becomes *Masha* and the end *Ira*. The mass is assigned according to the type of a randomly chosen bead (nm) using the code:

```

IF(who_are_you(nm).eq..TRUE.)THEN
mp = m4
ELSEIF(who_are_you(nm) .eq..FALSE.)THEN
mp = m3
ENDIF

```

(21)

The probability for this update is given by

Glue/Close Update

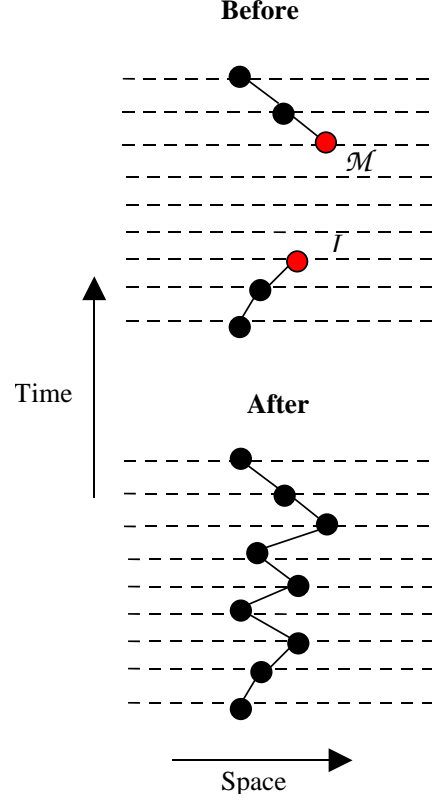


FIG. 8: Worm Algorithm update for closing a worm to become a diagonal configuration.

$$P_{cut} = \min \left\{ 1, \frac{C\bar{M}N_{bd}e^{\Delta U - \mu M \epsilon}}{\rho_0(\mathbf{r}_I, \mathbf{r}_M, M \epsilon)} \right\}, \quad (22)$$

and is coded

$$P_{cut} = \frac{1}{4} e^{-\mu \epsilon M + \Delta U} e^{(\mathbf{r}_I - \mathbf{r}_M)^2 \cdot \frac{mp}{2\epsilon M}} (aM)^{3/2} \cdot N_{bd} \cdot w_{ST} \bar{M} \cdot \frac{p_{gl}}{p_{cut}} \cdot w_{lc, I} \cdot w_{lc, M} \cdot w_t \quad (23)$$

10. Reconnect Masha

In this swap update, *Masha* of an open world line (worm) and time slice j is connected to a randomly chosen bead α at time $j - M$ on another close world line (ring polymer) as shown in Fig.10, by building a new trajectory between *Masha* at time j and α at time $j - M$. Prior to this, the trajectory connecting α to a bead ξ , where ξ is in the same time slice as *Masha*, is removed. Again,

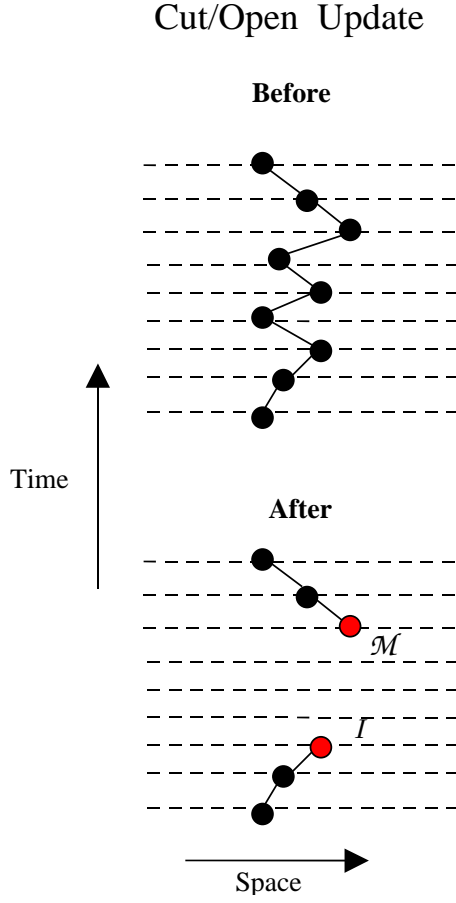


FIG. 9: As in Fig.8; but for cutting a ring polymer open, i.e., making a diagonal configuration off-diagonal.

the mass of each bead is chosen depending on the type of worm inserted in Sec.IIB2 and to be updated here. We made sure that the swap updates are done between the same type of beads as before:

IF(*who_are_you*(\mathcal{M})).**ne.***who_are_you*(α))**RETURN**
(24)

and throughout the removal of the trajectory (i.e., the beads say $\{bead1, bead2, bead3, \dots, beadM\}$ between ξ and $\alpha \equiv bead1$ one checks:

IF(*who_are_you*(*bead1*)).**ne.***who_are_you*(*bead2*))**STOP**
(25)

and similarly for the rest of the beads, where *bead2* = **next**(*bead1*), *bead3* = **next**(*bead2*) and so on (see [1]). Thus, if a bead does not have the same type as *Masha* the update is rejected. If the update is accepted, the previous ξ then becomes the new *Masha* and the old *Masha* is connected to α . The probability for this update is

$$P_{re,\mathcal{M}} = \min \left\{ 1, e^{-\Delta U} \frac{\Sigma_{\mathcal{M}}}{\Sigma_{\xi}} \right\}, \quad (26)$$

where

$$\Sigma_{\mathcal{M}} = \sum_{\sigma \in \mathcal{L}_{\mathcal{M}}} \rho_0(\mathbf{r}_{\mathcal{M}}, \mathbf{r}_{\sigma}, \overline{M}\epsilon), \quad (27)$$

and

$$\Sigma_{\xi} = \sum_{\sigma \in \mathcal{L}_{\xi}} \rho_0(\mathbf{r}_{\xi}, \mathbf{r}_{\sigma}, \overline{M}\epsilon), \quad (28)$$

with $\mathcal{L}_{\mathcal{M}}$ the list of particles in the slice $j - M$ in the bins that spatially coincide with the bin of *Masha* or one of its nearest neighbors, similarly for \mathcal{L}_{ξ} .

The swap probability for *Masha* is coded

$$P_{re,\mathcal{M}} = \frac{\Sigma_{\mathcal{M}}}{\Sigma_{\xi}} \frac{w_{lc,\mathcal{M}}}{w_{lc,\xi}} w_t e^{-\Delta U} \quad (29)$$

with

$$\Sigma_{\mathcal{M}} = \left(\frac{1}{\sqrt{aM}} \right)^3 \sum_{i=1}^{h_m} e^{-(\mathbf{r}_{\mathcal{M}} - \mathbf{r}_i)^2 \frac{mp}{2\epsilon M}}, \quad (30)$$

and

$$\Sigma_{\xi} = \left(\frac{1}{\sqrt{aM}} \right)^3 \sum_{i=1}^{h_m} e^{-(\mathbf{r}_{\xi} - \mathbf{r}_i)^2 \frac{mp}{2\epsilon M}}. \quad (31)$$

Here h_m is the number of particles in $\mathcal{L}_{\mathcal{M}}$ and (in the next section) in \mathcal{L}_{ξ} .

11. Reconnect Ira

This is a swap update as in the previous section but for *Ira* as shown in Fig.11. The probability for this update is given by

$$P_{re,\mathcal{I}} = \min \left\{ 1, e^{\Delta U} \frac{\Sigma_{\mathcal{I}}}{\Sigma_{\xi}} \right\}, \quad (32)$$

where

$$\Sigma_{\mathcal{I}} = \sum_{\sigma \in \mathcal{L}_{\mathcal{I}}} \rho_{\sigma}(\mathbf{r}_{\mathcal{I}}, \mathbf{r}_{\sigma}, \overline{M}\epsilon), \quad (33)$$

and Σ_{ξ} was given by Eq.(31) previously. The probability for this update is coded:

Reconnect Masha Update

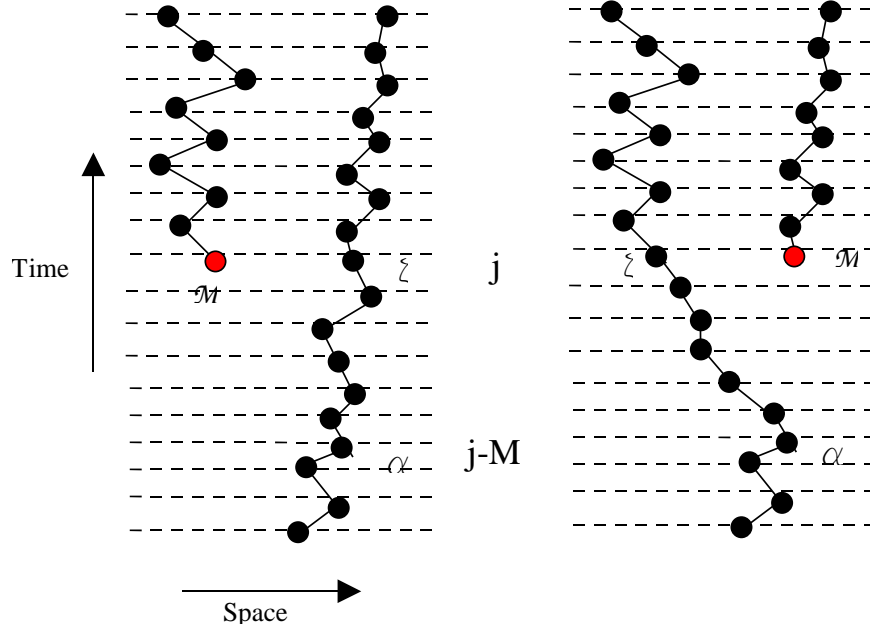


FIG. 10: Worm-Algorithm swap updates: After cutting a piece of trajectory between the beads α and ξ from the path to the right of \mathcal{M} , *Masha* is reconnected to bead α chosen randomly on the other path, and ξ becomes the new *Masha*.

$$P_{re,\mathcal{I}} = \left(\frac{1}{\sqrt{a\bar{M}}} \right)^3 \frac{\sum_{\mathcal{I}} w_{lc,\mathcal{I}}}{\sum_{\xi} w_{lc,\xi}} e^{\Delta U} w_t \exp(\Delta U). \quad (34)$$

Again, one makes sure that the swap updates are done on the same type of beads:

$$\mathbf{IF}(who_are_you(\mathcal{I}).ne.who_are_you(\alpha))\mathbf{STOP}, \quad (35)$$

and during the removal of the path between α and ξ

$$\mathbf{IF}(who_are_you(bead1).ne.who_are_you(bead2))\mathbf{STOP}. \quad (36)$$

12. Insert Link

In addition to the previous updates, this update creates a bond (diagrammatic link) between the beads. In Fig.12, a bond (link) is created between beads a_i and b_i and the probability for this update is given by:

$$P_{crb} = \frac{(\bar{M} + 1) n_B}{(\ell_{bnd} + 1) P_{AB}} \left(e^{-fu(\mathbf{r}_{a_j} - \mathbf{r}_{b_j})} - 1 \right), \quad (37)$$

where, $u(\mathbf{r}_{a_j} - \mathbf{r}_{b_j})$ is the interaction potential between beads a_j and b_j , n_B is the number of beads in a spatial bin \mathcal{B} within the slice j of the bead a_j , where the update will be given a try, ℓ_{bnd} is the total number of bonds in the initial configuration, and P_{AB} is a probability that depends on the distance between bins \mathcal{B} and \mathcal{A} . The probability is encoded

$$P_{crb} = pat \cdot (e^{-fu(\mathbf{r}_{a_j} - \mathbf{r}_{b_j})} - 1) \frac{\bar{M} + 1}{n_{li} \cdot prob(evk)} \quad (38)$$

where n_{li} is the total number of links, pat the number of beads n_B , $prob(evk)$ is P_{AB} . Again, the type of bead to which a link is created doesn't matter. So, we do not check here whether two beads to be linked have the same type or not.

13. Remove Link

This update removes a bond between beads a_i and b_i , as shown in Fig.13. The probability for this update is given by

$$P_{rmb} = \frac{\ell_{bnd} P_{AB}}{(\bar{M} + 1) n_B} \left(e^{-fu(\mathbf{r}_{a_j} - \mathbf{r}_{b_j})} - 1 \right)^{-1}. \quad (39)$$

Reconnect Ira Update

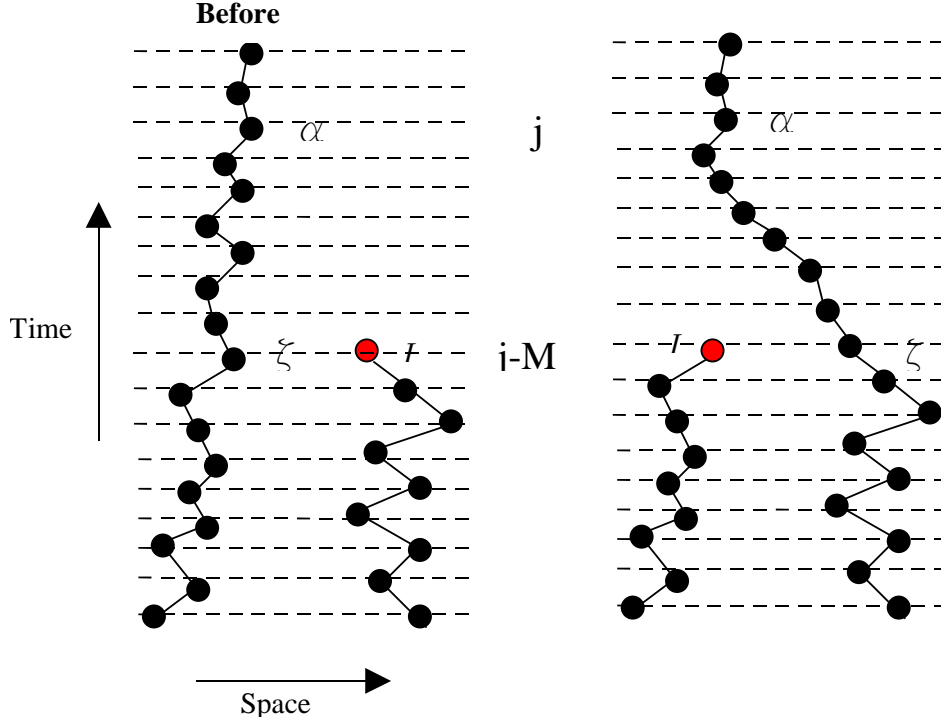


FIG. 11: Worm Algorithm swap update: *Ira* is reconnected to α after removing the trajectory between ξ and α . ξ is at the same time as *Masha*.

14. Diagonal

In this update, a randomly chosen piece of trajectory is removed from a closed path and replaced by a newly generated trajectory, as shown in Fig.14. The probability for this update is given by

$$P_{diag} = e^{-\Delta U}. \quad (40)$$

The newly generated trajectory must have the same type as the initial diagonal configuration, otherwise the update is rejected.

C. Mobility of ^3He in ^4He

There is an inherent difficulty in the diffusion of ^3He atoms in bulk ^4He . To increase the mobility of ^3He inside ^4He , we applied an approach invented by previous authors [15], which makes use of the concept of a fictitious or fake particle. On the other hand, this method also addresses the diffusion of ^4He atoms in the system. In this technique, one introduces into the system a fake ^3He or ^4He particle whose mass is allowed to vary during the simulation in increments of $\pm dm$. One can then

increase the mobility of ^3He and ^4He atoms by reducing their mass or vice versa.

Computationally, an array *markf* is introduced in order to mark beads as either fake (**.FALSE.**) or real (**.TRUE.**). This array is initialized in the beginning to **.TRUE.**. Next, two mass differences

$$\begin{aligned} \Delta m_3 &= |m_{fake} - m_3| \\ \Delta m_4 &= |m_{fake} - m_4| \end{aligned} \quad (41)$$

determine whether a fake ^3He or ^4He atom of mass m_{fake} is to be chosen. The mass m_{fake} is initialized to m_3 and then updated by a subroutine as explained below. If $|\Delta m_3| < dm$, where $dm = (m_4 - m_3)/10.$, a subroutine choosing a fake ^3He particle is called. Otherwise, if $|\Delta m_4| < dm$, another subroutine chooses a fake ^4He particle (see Appendix). When a fake particle is chosen, the beads of its closed trajectory are labelled **.FALSE.**

1. Choosing a fake ^3He particle

In the subroutine choosing a fake ^3He particle, a bead (*bead1*) is selected randomly from a list of beads [*nlist()*]:

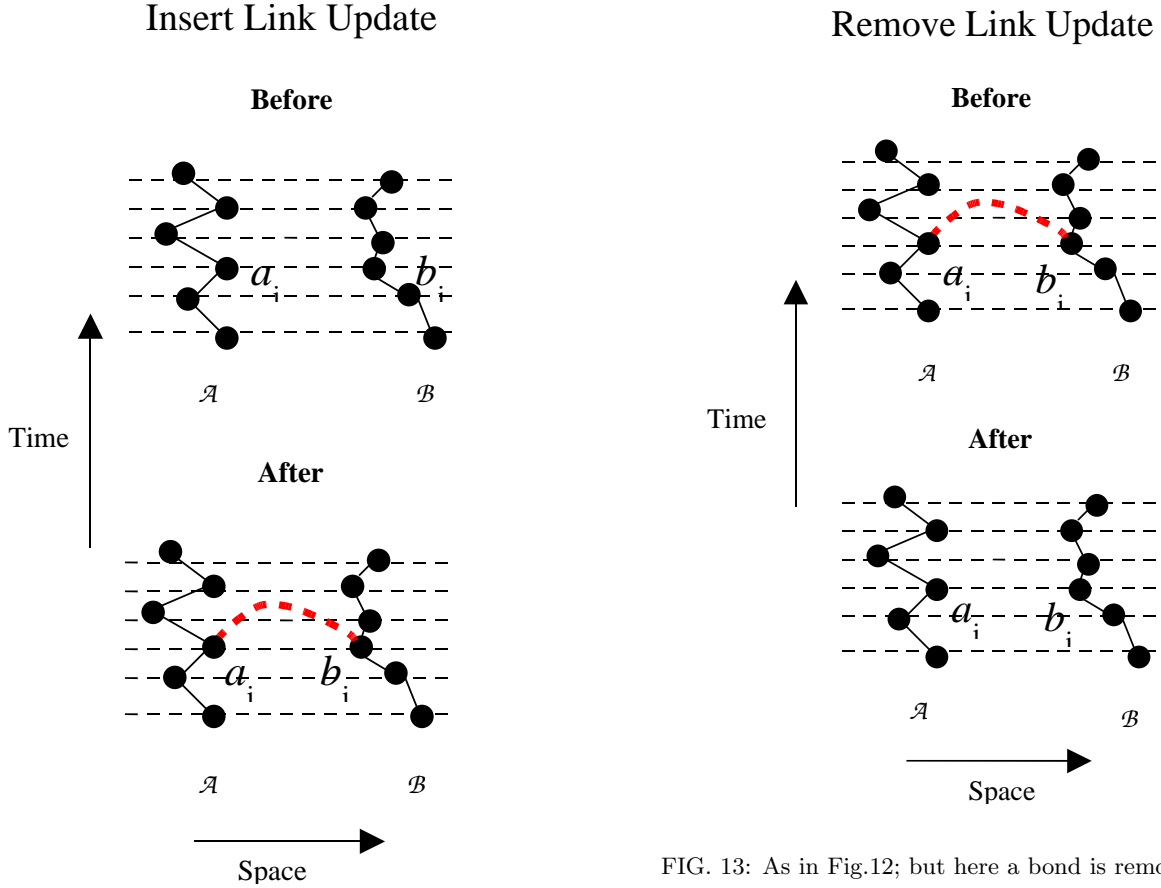


FIG. 13: As in Fig.12; but here a bond is removed.

FIG. 12: Insert link update: A bead is created between randomly chosen beads a_j and b_j on different world lines and in the same time slice in their spacial bins \mathcal{A} and \mathcal{B} , respectively.

$$i = \text{rndm}() * \text{nmnm} + 1; \quad ip = \text{nlist}(i); \quad \text{bead1} = ip, \quad (42)$$

where nmnm is the number of beads at some number of Monte Carlo steps. If it happens that (bead1) is a ${}^3\text{He}$ atom, a trajectory of length $\beta = \text{Mbeta}$ time slices is assigned using a bead-list array $\text{lbfnw}()$ starting with $\text{lbfnw}(0) = \text{bead1}$. Otherwise, if bead1 is ${}^4\text{He}$, the routine returns to (42) above and tries again until a ${}^3\text{He}$ bead1 is chosen. If the last bead ($ip = \text{lbfnw}(\text{Mbeta})$) is not equal to bead1 , that is the particle is in an exchange cycle, the chosen fake trajectory is rejected, i.e., its beads are not relabelled **.FALSE.**. The subroutine then returns to Eq.(42) and starts all over again. If all goes well, that is by having a fake and closed pure ${}^3\text{He}$ or ${}^4\text{He}$ trajectory, a loop labels the beads of the chosen trajectory by **.FALSE.** to make it fake:

```

markf = .TRUE.
do   k = 0, Mbeta
lbfnw(k) = lbfnw(k)
markf(lbfnw(k)) = .FALSE.
enddo
(43)

```

The subroutine choosing a fake ${}^4\text{He}$ particle is exactly the same, except for ${}^4\text{He}$. This subroutine is called when $\Delta m_4 \leq dm$, i.e., when mfake has reached the mass of ${}^4\text{He}$ during the mass update described next. Once a fake trajectory is chosen, its mass is updated by a subroutine for changing the mass of the fake particle. Physical properties are then measured when $|\Delta m_3| \leq dm$ or $|\Delta m_4| \leq dm$. Hence, any trajectory which has $\Delta m_3 < dm$ or $\Delta m_4 < dm$ is considered real and can be used to measure physical properties in a given particle number sector. Thus when $\Delta m_3 < dm$, the routine looks for another ${}^3\text{He}$ atom to put the fake label on, i.e., one looks for the bead which is the same as the current fake, not in exchange cycles and not fake. Once this bead is found, the previous fake labels are dropped and given to the new bead upon which a whole new closed trajectory is labelled fake to which this beads belongs. Similarly, when $\Delta m_4 < dm$, the same procedure is applied, except that one chooses a fake ${}^4\text{He}$ atom. A fake atom

Diagonal Update

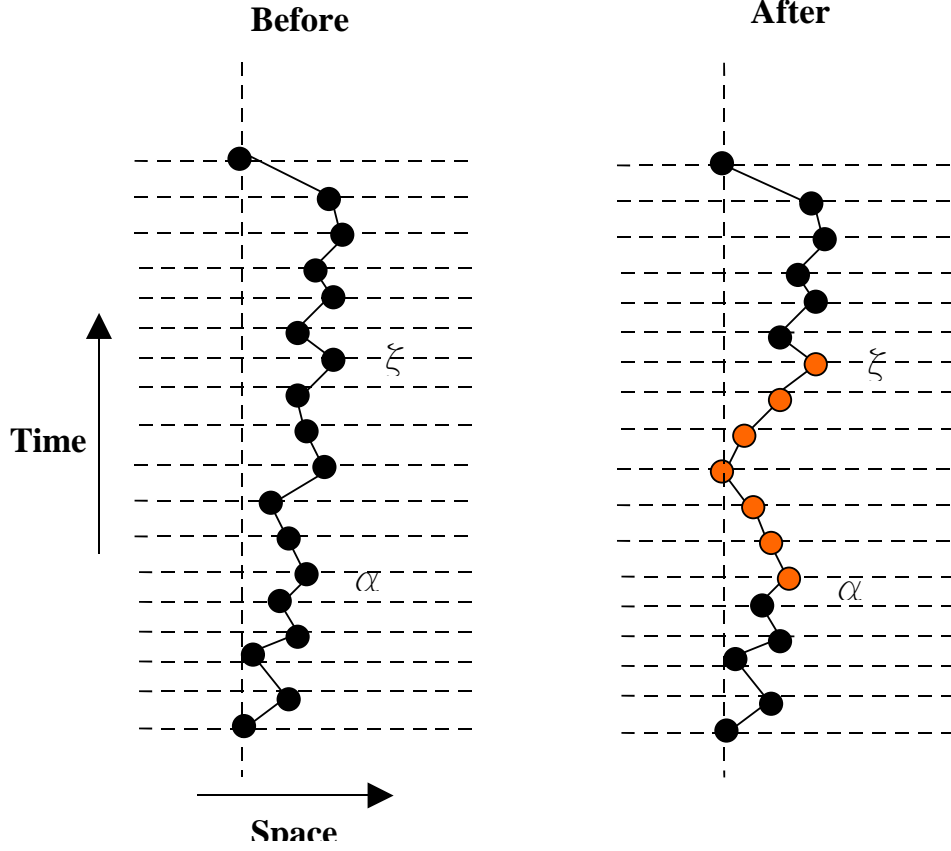


FIG. 14: Worm Algorithm Diagonal update where a piece of a trajectory is replaced by another one, necessarily of the same type of beads.

is not introduced when a worm is present. That is, one cannot perform these updates on worms, and one cannot have a fake worm. We must nevertheless emphasize that there will always be one fake atom in the configuration, it never disappears. And this fake atom is not part of any exchange cycle.

2. Mass update

Once a fake trajectory has been selected, its mass is updated using a subroutine (see Appendix) that we wrote for this following Ref.[15]. In this subroutine, the trajectory mass is incremented or decremented in steps of dm , that is,

$$m_{fake} = m_{old} + sgn * dm, \quad (44)$$

where the sign of the increment, $sgn = \pm 1$, is chosen

randomly by the mechanism

$$\begin{aligned} x &= rndm() \\ sgn &= (-1) * (int(2. * x)), \end{aligned} \quad (45)$$

and m_{old} is the fake (old) mass from the previous update. Thus m_{fake} is constantly updated until it becomes either m_4 or m_3 within a small margin of error $|\Delta m_3| < dm$ or $|\Delta m_4| < dm$. In this case, the mass update stops momentarily allowing a measurement of physical properties. Then, a new fake trajectory is selected. We need to emphasize that the previous trajectory is reset to real (**.TRUE.**) before either one of the subroutines for choosing a fake is called again. That is, no more than one fake trajectory is allowed. Further, inside the subroutine for choosing a fake mass, its mass is not allowed to obtain values less than m_3 or larger than m_4 . If it reaches one of them, the mass update is rejected and m_{fake} is reset to m_{old} . That is m_{fake} must always remain in the interval $[m_3, m_4]$. The mechanism by which the mass update in Eq.(44) is accepted or rejected is according to a certain

probability given by

$$P = \exp[\ell_k \Delta m / (2\epsilon)] \cdot \exp[\alpha(m \pm \Delta m)] / \exp[\alpha m], \quad (46)$$

which is actually a modified version of that of Corboz *et al.* [15] and which proved suitable for our purposes. Here ℓ_k is defined as

$$\ell_k = \sum_{k=1}^M (\mathbf{r}_k - \mathbf{r}_{k-1})^2, \quad (47)$$

and α is an adjustable parameter. According to this probability, if $P < 1$ and $P > \xi$, where ξ is a random number, the mass update is rejected and the newly proposed fake mass in (44) is set back to the previous one, $m_{fake} = m_{old}$. Otherwise, m_{fake} is assigned the newly proposed value.

3. Mass histogram

During the above processes, statistics for a mass histogram for the several fake particles are collected in 10 mass bins as was done in Ref.[15]. This is in order to make sure that the different 10 mass intervals are addressed with almost the same probability. For this purpose, one tunes the α value above such that one gets an almost mass flat histogram.

III. RESULTS AND DISCUSSION

In this section, we present the results of our simulations. We display the pair correlation function $g(r)$ for the three different temperatures $T = 30, 40,$ and 50 mK, noting that the correlations weaken as the temperature is reduced to 30 mK. Next, the Matsubara Green's function [1, 18] reveals the presence of a condensate fraction in the system, whereas the ^3He component completely depletes the superfluid. In what follows, we first outline the difficulties which restricted our investigations to only three temperatures.

A. Difficulties in the WAQMC Simulations

It was possible to conduct WAQMC simulations on three milli-Kelvin temperatures only. The reasons are as follows. First, in order to reach the milli Kelvin regime $T < 100$ mK, one needs to use a large number of “time” slices β given by $M = \beta/\tau$. For our present purposes, we used a time step of $\tau = 1/400 \text{ K}^{-1}$ and a simulation box of dimensions $19.693 \text{ \AA} \times 17.054 \text{ \AA} \times 26.798 \text{ \AA}$. For example, for $\beta = (1/0.04) \text{ K}^{-1}$ and $\tau = (1/400) \text{ K}^{-1}$, one needs $M = 10000$. This is a very large number of time slices for WAQMC, let alone PIMC. Until now, and

to the best of our knowledge, no one has ever conducted PIMC calculations below 250 mK because of the considerable computational cost involved. Nevertheless, we decided to take this step to explore the physics of the current system in this difficult regime.

Second, because we used a repulsive statistical potential [19] for the ^3He pair interaction, the probabilities for worm updates on the ^3He system were lowered substantially (as one can see by inspecting the worm-update probabilities in Sec.IIB, which are governed by the interaction of a worm with the rest of the system). Consider further the substantial large number of ^3He atoms present in the current system which provides a large repulsive interaction energy. As a result, the evolution of the current simulated system took a considerable computational time in order to reach thermal equilibrium. The fact that the use of repulsive potentials in the WAQMC method can render the simulation inefficient was already mentioned by Boninsegni *et al.* [23]. In other words, under these circumstances, the worm updates occur at a significantly lower rate.

Third, the exact adjustment of the chemical potential μ posed another challenge. The average number of particles $\langle N \rangle$ is allowed to vary by running the WAQMC simulation in the grand canonical ensemble. When the system eventually thermalizes, the number of particles, as determined by μ , stabilizes after a long run or thermal evolution time. It is very difficult to predict the number of particles to which the system would eventually thermalize by guessing μ from the outset, i.e., the beginning of a simulation. One can only conduct several runs at different μ and the same T in order to obtain various numbers of particles corresponding to the chemical potentials used. Then, one can construct a “calibration curve” of $\langle N \rangle$ vs. μ for each T within an acceptable error range of $\langle N \rangle$. That way μ can be predicted – numerically speaking – more reliably for other nearby temperatures. Yet, this procedure is very time-consuming, given that one needs to wait for the system to thermalize for each value of μ chosen. It could take months to determine the correct μ with the computational resources that we have currently available. As a result, we chose to conduct a *qualitative* investigation of this system by running the WAQMC simulations in the *canonical ensemble* by choosing a reasonable μ . In fact, it was later found that in the milli-Kelvin temperature regime, N turns out to be independent of μ .

B. Pair correlations

The correlation function $g(r)$ counts the number of atom pairs with interparticle distance r . It provides evidence for the clusterization of particles around certain locations in the system. Fig. 15 displays correlation functions for our system at the indicated temperatures: 50 mK (open circles); 40 mK (solid circles); 30 mK (open triangles). The peaks in this figure strongly indicate the

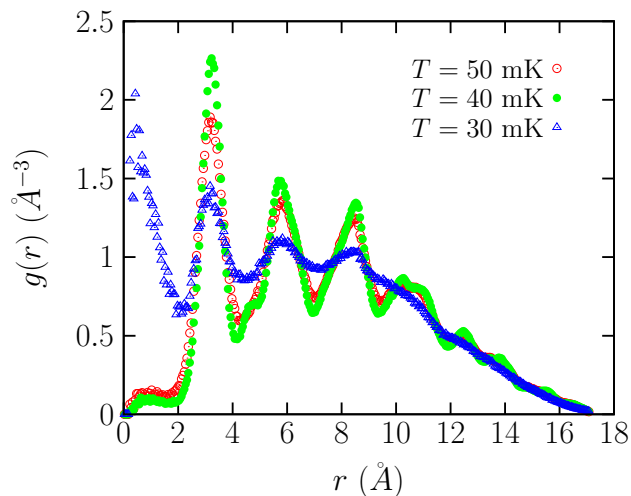


FIG. 15: WAQMC pair correlation function $g(r)$ for the ${}^4\text{He}$ - ${}^3\text{He}$ system at three different temperatures: $T = 30$ mK (open circles); 40 mK (solid circles); and 30 mK (open triangles). Distances are in units of Å , and $g(r)$ is in units of Å^{-3} .

presence of clusters –possibly droplets. This explanation is similar to that given by Boninsegni and Szybisz [24], who investigated helium films on lithium substrates at $T = 0.5$ K. Their $g(r)$ acquires a nonzero value at the origin, indicating that the helium film is forming droplets on the substrate surface. Inspecting Fig. 15, one can see that $g(r = 0) = 0$ at all T . That is, the ${}^4\text{He}$ adsorbed on the substrate forms no droplets, as it is almost a solid. The rest of the peaks in $g(r)$ possibly signals the presence of pure ${}^4\text{He}$ clusters at $r \sim 3\text{Å}$, ${}^3\text{He}$ - ${}^4\text{He}$ (pair) clusters at $r \sim 6\text{Å}$, and pure ${}^3\text{He}$ - ${}^3\text{He}$ (pair) clusters at $r \sim 8\text{Å}$. This is a reflection of the zero-point motion of ${}^3\text{He}$ and ${}^4\text{He}$, that of ${}^3\text{He}$ being larger, of course. Accordingly, the pure ${}^4\text{He}$ cluster would have the lowest interparticle distances around $r \sim 3\text{Å}$. The ${}^3\text{He}$ - ${}^4\text{He}$ cluster would have larger interparticle distances because of the larger ${}^3\text{He}$ zero-point motion. Finally, the ${}^3\text{He}$ cluster has the largest interparticle distances as it is undergoing only ${}^3\text{He}$ zero-point motion. Yet $g(r)$ in Fig. 15 decays to zero at large $r \geq 16\text{Å}$, the reason being that our system is simulated in a box of finite size and does not extend to infinity. There are some remaining oscillations in $g(r)$ at $r \geq 10\text{Å}$, which could be indicative of other types of structures. However, at $T = 30$ mK, $g(r)$ has a peak at $r \sim 0.5\text{Å}$. Some particles may have left the higher layers and approached the graphite surface, most likely ${}^3\text{He}$. Being attracted by the strong graphite potential, once the ${}^3\text{He}$ atoms reach the surface of the substrate, the strong ${}^3\text{He}$ -graphite interaction (~ -200 K) overcomes their zero-point motion (~ 7 K), and they begin to form more ${}^3\text{He}$ or ${}^3\text{He}$ - ${}^4\text{He}$ clusters close to the surface. Further, the intensity of $g(r)$ at $r \sim 3, 6,$ and 8Å indicates clustering closer to the graphite surface, as atoms leave the higher layers and approach the substrate.

A question arises as to the role of temperature reduc-

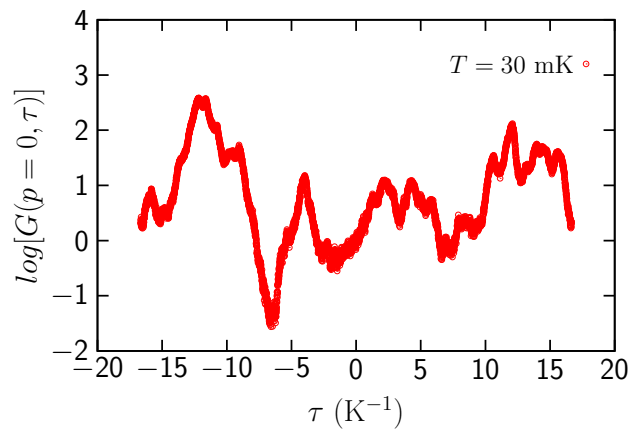


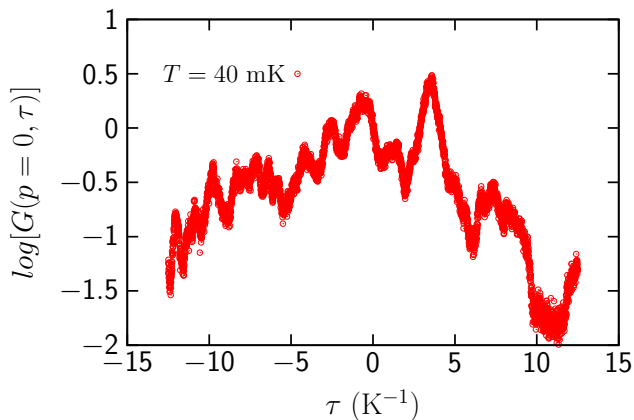
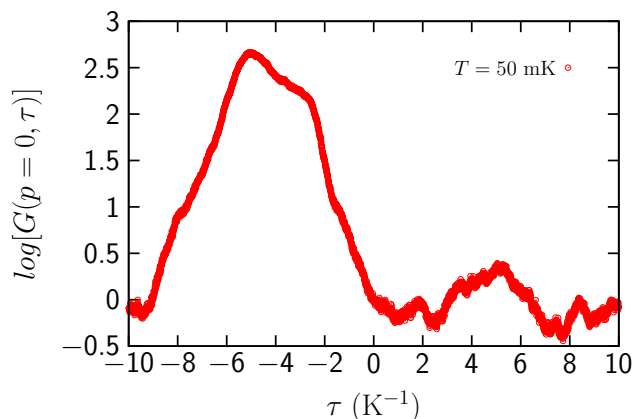
FIG. 16: The logarithm of the WAQMC zero-momentum Matsubara Green function $\log[G(p = 0, \tau)]$ at $T = 30$ mK. The “time” τ is in units of K^{-1} .

tion on particle promotion and demotion from one layer to another. Are ${}^3\text{He}$ atoms (or ${}^4\text{He}$) being demoted from the highest layer down, closer to the graphite surface? What is the role of the statistical potential in this case? We know that it is temperature-dependent.

C. Matsubara Green’s function

In what follows, we explore the possibility for the presence of excitations in the system by measuring the Matsubara Green’s function (MGF) $G(p, \tau)$ [18] at zero momentum using WAQMC. In other words, we check whether our system, as simulated by WAQMC, has really reached its ground state or not. This is a crucial point in the verification of the reliability of the results. Often, in heavy computational techniques like WAQMC, such a step can give the green light for finally stopping the simulation.

Figs. 16, 17, and 18 present the WAQMC $G(p = 0, \tau)$ at $T = 30, 40,$ and 50 mK in the “time” range $-\beta \leq \tau \leq \beta$. The $G(p = 0, \tau)$ signal significant activity in the system at the various times τ . The particles seem to propagate at various amplitudes of the MGF in the $p = 0$ state at the different values of τ ; yet no signals for particle excitations or deexcitations are detected. In fact, the Green function at $\tau = 0$ corresponds to the number of particles in the condensate N_0 ! That is, according to Mahan [18], $G(p = 0, \tau = 0) \propto -N_0$, where the proportionality sign arises because the Green function obtained in this treatment contains signals from both the fermions and the bosons. Accordingly, one might be tempted to argue that there is a condensate in our system since, at $\tau = 0$, the Green function in all three Figs. 16, 17, and 18 displays a nonzero value.

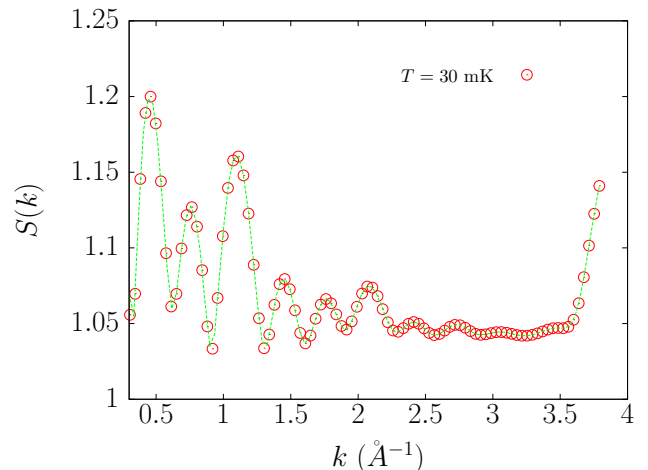
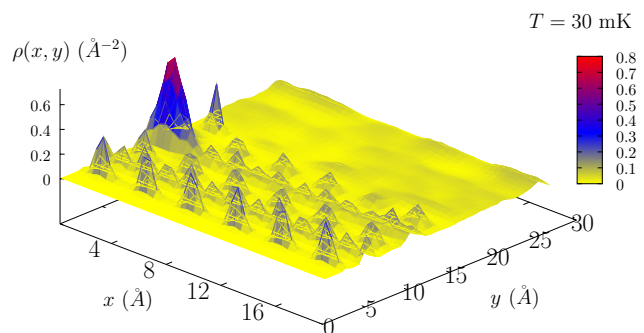
FIG. 17: As in Fig. 16; but for $T = 40$ mK.FIG. 18: As in Fig. 16; but for $T = 50$ mK.

D. Structure Factor

Fig. 19 displays the static structure factor $S(k)$ for the sandwich system at $T = 30$ mK. Three significant Bragg peaks appear at $k \sim 0.5, 0.75,$ and 1.2 \AA^{-1} , which reveal crystalline order in the system, largely present in the first few ^4He layers closest to the graphite substrate. The strong attraction of the helium atoms to the graphite forces crystalline order as the ^4He atoms get adsorbed on the substrate surface. The absence of Bragg peaks in the higher layers is a consequence of the He-graphite potential becoming weaker. As a result, the bulk ^3He component is completely disordered.

E. Density Profiles

Figures 20-22 display integrated two-dimensional profiles at $T = 30, 40,$ and 50 mK, respectively, in the $x - y$ plane perpendicular to the graphite surface $x - z$. The integration is performed along the z -axis. A peculiar density distribution is observed at 30 mK, where

FIG. 19: WAQMC static structure factor $S(k)$ at $T = 30$ mK. The quasi-momentum wave vector k is in units of \AA^{-1} .FIG. 20: Integrated density $\rho(x, y)$ at $T = 30$ mK along the z -axis in the xy plane perpendicular to the graphite substrate plane

there is a high peak observed (red cusp), indicating clusterization of the helium atoms. However, it is difficult to tell whether these would be ^3He or ^4He (or both) clusters. Further, there is a smooth, slightly wavy area in the xy plane at $20 \leq y \leq 30 \text{ \AA}$ where a crystal structure seems to be absent, and may possibly indicate the presence of a liquid. Figure 21, on the other hand, does not reveal any signals for clusterization at 40 mK. The sharp, periodically ordered peaks are indicative of a largely prevalent crystalline structure. Figure 22 reveals the same absence of crystallization.

IV. CONCLUSIONS

In summary, then, the thermal and structural properties of the ^3He - ^4He system were investigated at low temperatures in the milli-Kelvin regime. These temperatures lie in an extremely difficult regime in which WAQMC runs must take a long time so as to give good results. The correlations, structure factor, Matsubara Green's func-

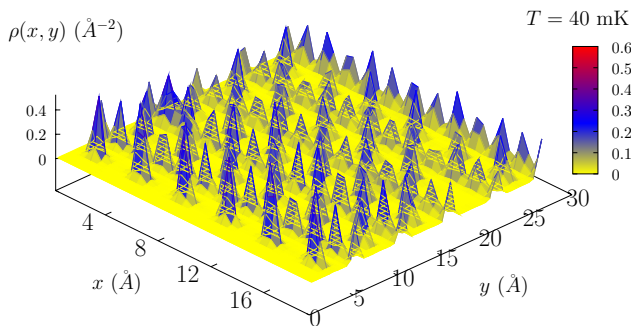


FIG. 21: As in Fig. 20; but for 40 mK.

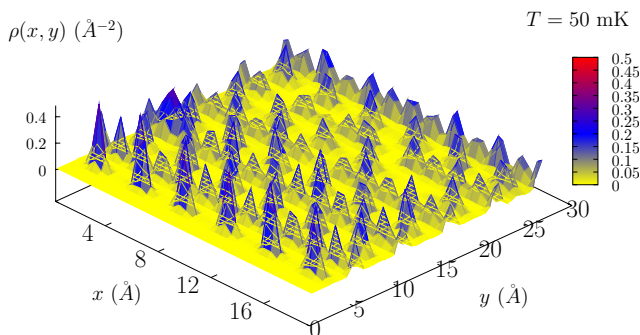


FIG. 22: As in Fig. 20; but for 50 mK.

tion, and density profiles were explored. A major point in this study is that we used a repulsive statistical potential in order to describe the ^3He atoms as real fermions. Although this potential slowed down the evolution of the system during the WAQMC calculation –that is, the ac-

ceptance probability of worm-updates was reduced and occurred less frequently than when using attractive interactions for the ^3He atoms – we were still able to evaluate the properties of the system.

It was found that the superfluid fraction of the sandwich has zero value. This is because the large number of ^3He atoms depletes the superfluid strongly. The correlation function of the system was evaluated at different temperatures. It was found to display three peaks at $r \sim 3, 6,$ and 8\AA , signalling $^4\text{He}-^4\text{He}$, $^4\text{He}-^3\text{He}$ and $^3\text{He}-^3\text{He}$ clusterizations, respectively. The structure factor was then investigated at $T = 30\text{ mK}$. It shows a quasicrystalline structure up to $k \sim 2.5\text{\AA}^{-1}$; but then disorder sets in. Three significant Bragg peaks appear at $k = 0.5, 0.75,$ and 1.2\AA^{-1} . The density profile of the system was explored at different temperatures. It was shown to depend strongly on temperature. Furthermore, at $T = 30\text{ mK}$, there is a clustering of the ^3He atoms in some region indicated by the highest peak in Fig. 20. In the future, we will explore a few ^3He atoms placed on a layer of ^4He atoms adsorbed on graphite using the same WAQMC code modified here.

Acknowledgments

We are very indebted for Nikolay Prokofev for providing us with his Worm Algorithm code. We would also like to thank him for his help in the modification of the code for the present purpose, and for enlightening and stimulating discussions. One of the authors (HBG) is grateful for The University of Jordan for granting him a sabbatical leave during which this work was completed. This research has been generously supported by the University of Jordan under project number 74/2008-2009 dated 19/8/2009..

-
- [1] M. Boninsegni, N. V. Prokof'ev, and B. V. Svistunov, Phys. Rev. E **74**, 036701 (2006).
 - [2] Humam B. Ghassib and Yahya F. Waqqad, Physica B **194-196**, 511 (1994).
 - [3] D. McQueeney, G. Agnolet, and J. D. Reppy, Phys. Rev. Lett. **52**, 1325 (1984).
 - [4] H. Akimoto and R. B. Hallock, Physica B **329-333**, 164 (2003).
 - [5] H. Akimoto, J. D. Cummings, and R. B. Hallock, Phys. Rev. B **73**, 012507 (2006).
 - [6] F. Ziouzia, J. Nyéki, B. Cowan, and J. Saunders, Physica B **329-333**, 252 (2003).
 - [7] A. Nash, M. Larson, J. Panek, and N. Mulders, Physica B **329**, 160 (2003).
 - [8] H. B. Ghassib, Z. Phys. B-Cond. Matt. 56 **56**, 91 (1984).
 - [9] M. Pierce and E. Manousakis, Phys. Rev. B **59**, 3802 (1999).
 - [10] Marlon Pierce and Efstratios Manousakis, Phys. Rev. B **63**, 144524 (2001).
 - [11] E. Krotscheck, J. Paaso, M. Saarela, and K. Schörkhuber, Phys. Rev. B **64**, 054504 (2001).
 - [12] H. B. Ghassib and S. Chatterjee, Proc. 17th Int. Conf. Low. Temp. Phys. Part II, 1241 (1984).
 - [13] D. McQueeney, Ph.D. thesis, Cornell University, New York (1988), (unpublished).
 - [14] Humam B. Ghassib and Yahya F. Waqqad, Physica B **165-166**, 595 (1990).
 - [15] Philippe Corboz, Massimo Boninsegni, Lode Pollet, and Matthias Troyer, Phys. Rev. B **78**, 245414 (2008).
 - [16] M. C. Gordillo and J. Boronat, Phys. Rev. Lett. **102**, 085303 (2009).
 - [17] S. Giorgini, J. Boronat, and J. Cassuleras, Phys. Rev. B **54**, 6099 (1996).
 - [18] Gerald D. Mahan, *Many-Particle Physics* (New York: Plenum, 1990), 2nd ed.
 - [19] R. K. Pathria, *Statistical Mechanics* (Butterworth-Heinemann, Jordan Hill, Oxford, 1996), second ed.
 - [20] R. A. Aziz, V. P. S. Nain, J. S. Carley, W. L. Taylor, and G. T. McConville, J. Chem. Phys. **70**, 4330 (1979).
 - [21] Nikolay Prokofev provided us with his Worm-Algorithm code used in Ref. above.
 - [22] D. M. Ceperley, Rev. Mod. Phys. **67**, 279 (1995).
 - [23] M. Boninsegni, N. V. Prokof'ev, and B. V. Svistunov, Phys. Rev. Lett. **96**, 070601 (2006).

[24] M. Boninsegni and L. Szybisz, Phys. Rev. B **70**, 024512 (2004).